

# Short Range Correlations and Spectral Functions in Asymmetric Nuclear Matter

P. Konrad, H. Lenske, U. Mosel

Institut für Theoretische Physik, Universität Gießen  
Heinrich-Buff-Ring 16, D-35392 Gießen, Germany

Dynamical correlations in asymmetric infinite nuclear matter are investigated in a transport theoretical approach. Self-energies due to short range correlations and their influence on the nucleon spectral functions are described in an approach accounting for a realistic treatment of mean-field dynamics and a self-consistently derived quasi-particle interaction. Landau-Migdal theory is used to derive the short range interaction from a phenomenological Skyrme energy density functional. The spectral functions in asymmetric nuclear matter are found to follow in their gross features closely the patterns observed previously in symmetric nuclear matter. An interesting sensitivity of dynamical self-energies and spectral functions on the momentum structure of the underlying interactions is found.

PACS numbers:

Keywords:

## I. INTRODUCTION

Correlations beyond those described by the static mean-field are of genuine interest for the understanding of the dynamics in a nuclear many-body system. Although experience seems to confirm the prevalence of mean-field dynamics and the directly related quasi-particle picture a closer inspection reveals that nucleons in matter obey more involved rules. For symmetric nuclear matter this has been discussed extensively in the literature, e.g. in a recent review [1], and also was considered in our previous work [2, 3, 4]. However investigations for asymmetric nuclear matter are rare. Some of the few cases are [5] and [7]. In symmetric matter and stable finite nuclei one finds typically a suppression of the quasi-particle strength by about 10%. Pure mean-field dynamics predicts that in nuclear matter the spin- and momentum states are uniformly occupied inside the Fermi sphere up to the sharp surface at the Fermi momentum  $k_F$ . Hence, the momentum distribution  $n_q(k)$  for protons and neutrons ( $q=p,n$ ), respectively, up to a normalization constant is described appropriately by a step function,  $n_q(k) \sim \theta(k_F^q - k)$  where  $k_F^p = k_F^n$  for symmetric nuclear matter. As a matter of fact, in a more realistic description, going beyond the mean-field, this pattern changes. The nucleons cease to be in sharp energy-momentum states but acquire spectral functions of a finite width, thus resolving the strict on-shell relation between energy and momentum. Hence, the mean-field configurations only exist with a finite life time, determined by the strength of the coupling to  $2h - 1p$  and  $1p - 2h$  states, respectively. Correspondingly, in finite nuclei one observes a reduction of single particle spectroscopic factors when going away from the Fermi level. More dramatic effects are found in exotic nuclei. Leaving the valley of stability, the experiments [8, 9] and theory [10, 11] agree in observing strongly suppressed single particle probabilities already close to the Fermi level of neutron-rich nuclei.

Despite the fact that strongly asymmetric exotic nuclei are of central interest for modern nuclear structure physics, the contributions of short range correlations to asymmetric nuclear matter and finite nuclei is still a rarely touched problem in nuclear physics. Short range correlations play an important role for the understanding of nuclear matter as for example seen in the observed high energy tails of nuclear momentum distributions and form factors. Also, short range correlations play a decisive role in understanding the structure of finite nuclei, particle production in heavy ion collisions and astrophysical objects like supernovae. Since supernovae are highly asymmetric in isospin we need a more detailed knowledge of correlations in asymmetric matter beyond ordinary mean-field interactions.

Here, our main goal is to explore the interplay of mean-field dynamics and correlations in asymmetric nuclear matter. It is worthwhile to recall that in asymmetric matter isovector interactions are giving rise to strongly asymmetric Fermi energies for proton and neutrons. Hence, as an immediate consequence the available density of states of excited states changes, becoming increasingly different for proton and neutron configurations, respectively, with changing proton-to-neutron ratio. This a new aspect, clearly not accessible in the conventional approaches concentrating on symmetric nuclear matter.

From our previous work we know that the spectral functions in symmetric nuclear matter are determined by interactions of extremely short range which are very well approximated by point couplings, reproducing almost perfectly results from rather involved many-body calculations, e.g. in [12], both for cold [2, 3] and hot [4] symmetric matter at all densities. It is therefore tempting to extend the same transport theoretical approach to asymmetric nuclear matter. The fully microscopic approaches to correlations in asymmetric matter use either only BHF self-energies from particle-particle ladders in the T-matrix approach [5] or include in addition hole-hole scattering [6,

7], corresponding to 2h1p self-energies but neglecting the 2p1h contributions for particle states. We go beyond the previous work and consider in this paper both types of dynamical self-energies, thus obtaining a consistent description of particle and hole states. However, this is achieved to the expense on treating the mean-field (BHF) parts phenomenologically.

A fully self-consistent description as indicated e.g. for symmetric matter in [6] is beyond the intention of the present paper. Therefore, long-range mean-field effects are included by a Skyrme energy functional by which we account for the above mentioned change in the Fermi energies of protons and neutrons, respectively. The basic transport theoretical relations are summarized in section II and are extended to the general case of asymmetric nuclear matter. We also discuss the influence of charge asymmetry on the mean-field, affecting both the effective mass and the effective binding potentials in asymmetric matter. Landau-Migdal theory is used to estimate the matrix elements for the  $ppp^{-1}$ ,  $nnn^{-1}$ ,  $pnn^{-1}$  and  $npp^{-1}$  collisions by which the dissipation of spectral single particle strength is determined. Results of transport calculations for the spectral functions, self-energies and momentum distributions of protons and neutrons in asymmetric nuclear matter at various degrees of neutron excess are presented in section III. Finally we will close in section IV with a summary and an outlook.

## II. SPECTRAL FUNCTIONS IN ASYMMETRIC NUCLEAR MATTER

The underlying model for our calculations was presented in [2, 3] and used for calculations in cold ( $T = 0$ ) symmetric nuclear matter at saturation point density  $\rho_0$  and for finite temperature and high densities in [4]. At this point we restrict ourselves to a short summary of the formalism with a few changes in respect to asymmetric nuclear matter. For a more detailed calculation see [2, 3, 4].

The two-particle-one-hole (2p1h) and one-particle-two-hole (1p2h) polarization self-energies  $\Sigma^>$  and  $\Sigma^<$  for nucleons in nuclear matter are given by [13]:

$$\begin{aligned} \Sigma_q^{\gtrless} = & g \sum_{q'} \int \frac{d^3 k_2 d\omega_2}{(2\pi)^4} \frac{d^3 k_3 d\omega_3}{(2\pi)^4} \frac{d^3 k_4 d\omega_4}{(2\pi)^4} (2\pi)^4 \delta^4(k + k_2 - k_3 - k_4) \overline{|M_{qq'}|^2} \\ & \times g_{q'}^{\gtrless}(\omega_2, k_2) g_q^{\gtrless}(\omega_3, k_3) g_{q'}^{\gtrless}(\omega_4, k_4) \end{aligned} \quad (1)$$

where  $g = 2$  is the spin degeneracy. Compared to symmetric nuclear matter neutrons and protons occupy different Fermi spheres, which leads to different self-energies. In the asymmetric case one has to account for collisions with particles of the same kind (pp and nn) and for collisions with particles of different kind (pn and np). This explains the summation over the isospin  $q'$  in equation (1).

The one-particle correlation function  $g_q^{\gtrless}$  in equation (1) can be expressed in terms of spectral functions

$$\begin{aligned} g_q^<(\omega, k) &= ia_q(\omega, k)\theta(\omega_q - \omega), \\ g_q^>(\omega, k) &= -ia_q(\omega, k)(1 - \theta(\omega_q - \omega)), \end{aligned} \quad (2)$$

where  $\omega_q$  is the Fermi energy of the nucleons and  $\theta(\omega_q - \omega)$  the step function to account for the Fermi distribution in case of cold nuclear matter. The nonrelativistic spectral function for nucleons is found explicitly as,

$$a_q(\omega, k) = \frac{\Gamma_q(\omega, k)}{(\omega - \frac{k^2}{2m_q} - \Sigma_q^{mf} - \text{Re}\Sigma_q^{ret}(\omega, k))^2 + \frac{1}{4}\Gamma_q^2(\omega, k)}, \quad (3)$$

where  $\text{Re}\Sigma_q^{ret}(\omega, k)$  is the real part of the retarded self-energy, which can be calculated dispersively:

$$\text{Re}\Sigma_q^{ret}(\omega, k) = P \int \frac{d\omega'}{2\pi} \frac{\Gamma_q(\omega', k)}{\omega' - \omega} \quad (4)$$

The width  $\Gamma_q(\omega, k)$  is given by the imaginary part of the retarded self-energy,

$$\Gamma_q(\omega, k) = 2\text{Im}\Sigma_q^{ret} = i(\Sigma_q^>(\omega, k) - \Sigma_q^<(\omega, k)). \quad (5)$$

We introduce the asymmetry coefficient

$$\xi = \frac{\rho_p}{\rho} \quad (6)$$

which indicates the fraction of protons at a given total isoscalar nucleon density  $\rho = \rho_n + \rho_p$ . In a finite nucleus with charge number  $Z$  we have  $\xi = Z/A$ .

To see the influence of asymmetry we split the mean-field in proton and neutron contributions:

$$\Sigma_p^{mf} = \Sigma_{pp}^{mf} + \Sigma_{pn}^{mf} = \rho\xi u_{pp} + \rho(1-\xi)u_{pn} \quad (7)$$

$$\Sigma_n^{mf} = \Sigma_{nn}^{mf} + \Sigma_{np}^{mf} = \rho(1-\xi)u_{nn} + \rho\xi u_{np}. \quad (8)$$

$\Sigma_{pp}^{mf}$  and  $\Sigma_{np}^{mf}$  are generated by the proton background, which vanishes for pure neutron matter.  $\Sigma_{nn}^{mf}$  and  $\Sigma_{pn}^{mf}$  are generated by the neutron background. On the right hand side  $u_{pp}$  and  $u_{pn}$  are effective interactions averaged over the proton Fermi sphere for  $u_{pp}$  and the neutron Fermi sphere for  $u_{pn}$  in phase space. The same for  $u_{np}$  and  $u_{nn}$ .

One can easily see in equation (8) that there is no difference for neutrons and protons in case of symmetric nuclear matter ( $\xi = 0.5$ ) and one has not to distinguish between protons and neutrons. Going over to the asymmetric case the mean-field contributions split up, now protons and neutrons are distinguishable by their different dynamical laws. Absorbing the momentum dependent part of the mean-field up to second order in  $k$  into the kinetic energy term

$$\hbar^2 \frac{k^2}{2m} + \Sigma_q^{mf}(k, \rho) \cong \hbar^2 \frac{k^2}{2m_q^*} + U_q^{eff}(\rho) \quad (9)$$

leads to an effective mass  $m_q^*$  and an momentum-independent effective potential  $U_q^{eff}$ . Starting with symmetric matter, where the effective masses and effective potentials are the same, for  $p$  and  $n$ , respectively, the masses and potentials for nucleons of different isospin start to split up for asymmetric matter. As seen in equation (3) the mean-field contribution plays an important role for the spectral function's pole structure. Hence, we expect a separation of the proton and neutron quasiparticle peaks.

We account for mean-field effects in our model by means of a Skyrme energy density functional with parameters taken from the recent set of ref. [17]. By executing the variation with respect to the kinetic energy density  $\tau_q$  and the nucleon density  $\rho_q$ , where  $q = n, p$  one obtains for the effective mass and for the effective potential:

$$\frac{m_q}{m_q^*} = 1 + \frac{2m_q}{\hbar^2} \left( \frac{1}{8} [t_1(2+x_1) + t_2(2+x_2)]\rho \right. \quad (10)$$

$$\left. + \frac{1}{8} [t_2(2x_2+1) - t_1(2x_1+1)]\rho_q \right)$$

$$\begin{aligned} U_q^{eff} = & \frac{1}{4} t_0 [2(2+x_0)\rho - 2(2x_0+1)\rho_q] \\ & \frac{1}{24} t_3 \rho^\sigma [2(2+x_3)\rho - 2(2x_3+1)\rho_q] \\ & \frac{1}{24} \sigma t_3 \rho^{\sigma-1} [(2+x_3)\rho^2 - (2x_3+1)(\rho_p^2 + \rho_n^2)] \\ & \frac{1}{8} [t_1(2+x_1) + t_2(2+x_2)]\tau \\ & \frac{1}{8} [t_2(2x_2+1) - t_1(2x_1+1)]\tau_q \end{aligned} \quad (11)$$

where  $\rho$  is the total and  $\tau$  total kinetic density. The Skyrme parameters  $x_0, x_1, x_2, x_3, t_0, t_1, t_2, t_3$  and  $\sigma$  are given in table I.

In the numerical calculations we use an iterative approach. Starting with an initial choice for the widths, i.e the imaginary part of the self-energy, we calculate the spectral functions, which then serve as input for re-calculating the self-energies. These results are used as input for the next step of an iterative calculation, thus improving the results. The calculation is stopped, when the spectral functions are converged to a given accuracy. In the language of Feynman diagrams this approach corresponds to the summation of the sunset diagram to all orders [3].

### A. The Short Range Interaction

The former investigations were restricted to symmetric nuclear matter at saturation density. That highly symmetric situation simplifies the calculations because protons and neutrons are indistinguishable. Irrespective of the charge state, spectral functions and other observables can be related to the common Fermi energy of protons and neutrons. As pointed out before, in asymmetric matter the isovector mean-field changes the situation completely by introducing a relative shift of the proton and neutron Fermi surfaces, in addition to the changes from the differences in particle

$t_0$ ( $MeV \cdot fm^3$ )	-2490.23
$t_1$ ( $MeV \cdot fm^5$ )	489.53
$t_2$ ( $MeV \cdot fm^5$ )	-566.58
$t_3$ ( $MeV \cdot fm^{3+3\sigma}$ )	13803.0
$x_0$	1.1318
$x_1$	-0.8426
$x_2$	-1.0
$x_3$	-1.9219
$\sigma$	1/6
$W_0$ ( $MeV \cdot fm^5$ )	131.0

TABLE I: The parameters of the Skyrme SLy230a [17] interaction. The spin-orbit parameter  $W_0$  is included for completeness only.

number. Also, by following the shift of the equilibrium density with increasing asymmetry, here we have to have information on the value of  $|M_{qq'}|^2$  at changing total number densities. However, from our former work we expect that only the short range parts of the full in-medium  $NN$  interaction will be relevant.

An appropriate approach to investigate this aspect and, as an important side aspect, to test the consistency with the mean-field part of the model calculations we use Landau-Migdal theory [14]. Given an energy density functional  $\mathcal{E}(\rho)$  Landau-Migdal theory provides a way to calculate the corresponding residual 2-quasiparticle (2QP) interaction by second variation of  $\mathcal{E}(\rho)$  with respect to the various spin and isospin densities [14, 15]. Hence, for an intrinsically density dependent interaction the corresponding Landau-Migdal interaction includes various rearrangement terms which ensure to fulfill a number of important consistency relations [14]. These relations would be violated if the bare G-matrix interaction would be used instead, as e.g. in [5, 7].

For a Skyrme energy density functional the resulting parameters  $f_0(\rho)$ ,  $f'_0(\rho)$ ,  $g_0(\rho)$  and  $g'_0(\rho)$ , characterizing the interaction strength and density dependence in the spin-isospin  $S = 0, T = 0$ ,  $S = 0, T = 1$ ,  $S = 1, T = 0$ ,  $S = 1, T = 1$  s-wave  $ph$  interaction channels, are in fact derivable in closed form, e.g. [15]. According to the structure of the Skyrme energy density functional the Landau-Migdal parameters are constrained to monopole and dipole components.

However, these Skyrme values include short and long range interactions. The origin and nature of the various pieces cannot be identified directly. Here we are interested mainly in the short range parts. A simple but meaningful way to extract the short range parts is to identify the long range components with pion exchange. Consequently, we define the short range part of the interaction by subtracting from the interaction derived from the Skyrme energy density functional the (central part of) the pion exchange  $NN$  interaction. Hence, we use the central interaction obtained from pion exchange and include anti-symmetrization explicitly by means of the spin and isospin exchange operators  $P_{\sigma,\tau}$ , respectively, thus leading to

$$V_\pi(\vec{k}_1, \vec{k}_2) = -f_\pi^2 D_\pi(\vec{k}_1, \vec{k}_2) \vec{\sigma}_1 \cdot \vec{\sigma}_2 \vec{\tau}_1 \cdot \vec{\tau}_2 (1 - P_\sigma P_\tau) \quad , \quad (12)$$

which evidently can be arranged into

$$V_\pi(\vec{k}_1, \vec{k}_2) = \sum_{S,T=0,1} V_{ST}^{(\pi)}(\vec{k}_1, \vec{k}_2) (\vec{\sigma}_1 \cdot \vec{\sigma}_2)^S (\vec{\tau}_1 \cdot \vec{\tau}_2)^T \quad (13)$$

Above, the momentum space pion propagator is denoted by

$$D_\pi(\vec{k}_1, \vec{k}_2) = \frac{1}{(p^2 + m^2)} F(p^2) \quad (14)$$

including a monopole form factor with a cutoff  $\Lambda = 800 MeV/c$ . The 3-momentum transfer is in the t-channel  $\vec{p} = \vec{k}_2 - \vec{k}_1$  while in the u-channel we have  $\vec{p} = \vec{Q} = \vec{k}_2 + \vec{k}_1$ . Numerically, we use  $f_\pi \simeq 0.075$  which is the standard value for the pseudo-vector  $\pi NN$  coupling constant.

Hence, we cast the energy density functional into the form

$$E(\rho) = E_s(\rho) + E_\pi(\rho) \quad (15)$$

where  $E_s \equiv E - E_\pi$  is the short-range contribution. The long range pionic part  $E_\pi$  is given by a sum over the various spin and isospin transfer contributions as defined in eq.13. Formally  $E_\pi$  can be written as a sum over all spin-isospin

channels

$$E_\pi(\rho) = \frac{1}{2} \sum_{q,q'=p,n} \sum_{S,T=0,1} \int \frac{d^3 k_1}{(2\pi)^3} \int \frac{d^3 k_2}{(2\pi)^3} \Theta(k_F(q) - k_1) \Theta(k_F(q') - k_2) \times V_{ST}^{(\pi)}(\vec{k}_1, \vec{k}_2) \langle (\vec{\sigma}_1 \cdot \vec{\sigma}_2)^S (\vec{\tau}_1 \cdot \vec{\tau}_2)^T \rangle \quad (16)$$

although in spin-saturated nuclear matter only the  $S = 0$  are non-vanishing. In symmetric, i.e. isospin saturated, nuclear matter also the  $T = 1$  components will not contribute. The brackets indicate traces over spin and expectation values on isospin and the step functions constrain the momentum integrals to the proton and neutron Fermi spheres with Fermi momenta  $k_F(q)$ ,  $q = p, n$ , respectively.

Performing the variation with respect to the various spin and isospin densities we find in symmetric nuclear matter the set of Landau-Migdal parameters which in standard notation are

$$f_0^{(\pi)}(\rho) = -4\pi \frac{9}{4} N_0(k_F) \frac{f_\pi^2}{2k_F^2} Q_0(1 + \frac{m_\pi^2}{2k_F^2}) + f^{(r)}(k_F) \quad (17)$$

$$f_0'^{(\pi)}(\rho) = +4\pi \frac{3}{4} N_0(2k_F) \frac{f_\pi^2}{2k_F^2} Q_0(1 + \frac{m_\pi^2}{k_F^2}) \quad (18)$$

$$g_0^{(\pi)}(\rho) = +4\pi \frac{3}{4} N_0(k_F) \frac{f_\pi^2}{2k_F^2} Q_0(1 + \frac{m_\pi^2}{2k_F^2}) \quad (19)$$

$$g_0'^{(\pi)}(\rho) = 4\pi N_0(k_F) f_\pi^2 \left( \frac{1}{m_\pi^2} - \frac{1}{8k_F^2} Q_0(1 + \frac{m_\pi^2}{2k_F^2}) \right) \quad (20)$$

where  $Q_0(z) = \frac{1}{2} \ln(\frac{1+z}{1-z})$  is the Legendre polynominal of second kind for  $l = 0$ . A more detailed calculation is found in the appendix. In the  $S = 0, T = 0$  interaction channel an additional rearrangement term appears

$$f^{(r)}(k_F) = N_0(k_F) V_0^{(\pi)}(0,0) h(k_F/m_\pi) \quad (21)$$

where  $V_0^{(\pi)}(q, k)$  is the monopole component of the  $S = 0, T = 0$  ph-u-channel pion exchange interaction and

$$h(z) = \frac{(1 + 2z^2) \ln(1 + 4z^2) - 4z^2}{8z^4} \quad . \quad (22)$$

The Landau-Migdal parameters are pure numbers obtained by normalizing the interactions to the level density at the Fermi surface. We use  $N_0(k_F) = 2k_F M^*/(\pi\hbar)^2$ , leading to  $1/N_0 = 154 \text{ MeV fm}^3$  at the saturation point with  $k_F = 1.33 \text{ fm}^{-1}$ .

The short range components are defined by subtracting the pion contributions, e.g. in the  $(S = 0, T = 0)$  interaction channel:

$$f_0^{(s)}(\rho) = f_0(\rho) - f_0^{(\pi)}(\rho) \quad (23)$$

and  $f_0'^{(s)}$ ,  $g_0^{(s)}$  and  $g_0'^{(s)}$  are defined accordingly. The  $\ell = 0$  monopole Landau-Migdal Parameters for the full Lyon-4 interaction and the short range parameters after subtraction of the pion parts are displayed in Fig.2. While the pion contributions are small in the  $(S = 0, T = 1)$  and the  $(S = 1, T = 0)$  channels, the  $(S = 0, T = 0)$  and  $(S = 1, T = 1)$  gain additional strength, being attractive in the first and repulsive in the second case.

The short range components are obtained by subtraction of the pion part from the full Landau-Migdal parameters, e.g. in the  $S = 0, T = 0$  channel:  $f_0^s(\rho) = f_0(\rho) - f_0^{(\pi)}(\rho)$  and correspondingly for the other channels. The matrix element relevant for our calculations is defined from the  $pp$ ,  $nn$ ,  $np$  and  $pn$  spin-scalar and spin-vector amplitudes, respectively,

$$f_{q'q}(\rho) = f_0(\rho) + (-)^{q'-q} f_0'(\rho); \quad (24)$$

$$g_{q'q}(\rho) = g_0(\rho) + (-)^{q'-q} g_0'(\rho) \quad (25)$$

by averaging over the spin degree of freedom. For the isospin projection quantum numbers we use  $q = \pm \frac{1}{2}$  for neutrons and protons. Because of isospin symmetry we have  $f_{pp} = f_{nn}$  and  $f_{pn} = f_{np}$ , respectively. Hence, we define

$$\overline{M}_{q'q}(\rho) = \frac{1}{4} (f_{q'q}(\rho) + 3g_{q'q}(\rho)) \quad (26)$$

and averaging out the charge state dependence in a second step,

$$\overline{M}(\rho) = \sqrt{\frac{1}{2}(|M_{pp}(\rho)|^2 + |M_{pn}(\rho)|^2)} . \quad (27)$$

Results for  $\overline{M}_{pp}(\rho)$ ,  $\overline{M}_{pn}(\rho)$  and  $\overline{M}(\rho)$  are shown in Fig.3. While the short range interaction among equal particles varies only slowly with density, the proton-neutron interaction shows a strong density gradient, reminiscent to the known relations. At saturation density of symmetric nuclear matter,  $\rho = \rho_0 = 0.16 \text{ fm}^{-3}$  we find  $|\overline{M}(\rho_0)| = 341 \text{ MeV fm}^3$ . This value compares extremely well to the independently derived matrix element  $|\widetilde{M}| = 320 \text{ MeV fm}^3$  determined in our previous investigations [2, 3, 4] by adjusting the transport theoretical spectral functions to those from the many-body calculations of Benhar et al. [12]. This very gratifying agreement confirms the validity of our approach also for asymmetric matter. Moreover, with the derivation of the relevant interaction matrix element in a theoretically well justified approach we have gained predictive power in regions of total density  $\rho$  and for asymmetries  $\xi = \rho_p/\rho = Z/A \leq \frac{1}{2}$  which were inaccessible before.

### III. CORRELATIONS IN ASYMMETRIC NUCLEAR MATTER

#### A. Interactions and Dynamical Self-Energies

Spectral functions and the imaginary part of the self-energies have been calculated for nucleons in neutron-rich infinite nuclear matter in the transport theoretical approach outlined in the previous sections. Results will be displayed at the saturation density  $\rho_0 = 0.16 \text{ fm}^{-3}$  of infinite symmetric nuclear matter although with decreasing values of the asymmetry  $\xi$  the equilibrium point moves to smaller densities and finally disappears below a critical value of  $\xi$ . Our choice of the Lyon-4 parameter set [17] for the Skyrme energy density functional leads to an higher effective mass for protons than for neutrons in neutron-rich matter, i.e.  $m_p^*(\rho, \xi) > m_n^*(\rho, \xi)$  for  $\xi < \frac{1}{2}$ .

The averaged scattering amplitude was chosen according to eq.27, thus accounting for the variation of the average matrix element with density. In all calculations, the real part of the self-energy, which plays an important role for analyticity [2], was included by means of using eq.(4). By numerical reasons the spectral functions were calculated on energy and momentum grids  $(\omega, k)$  with  $-0.5 \text{ GeV} \leq \omega \leq +0.5 \text{ GeV}$  and  $0 \leq k \leq 1.5 \text{ GeV}/c$  which obviously leads to a lack of information on the behavior of the spectral functions at energies outside the region covered by the numerical grid. For being able to calculate the  $\text{Re}\Sigma_q$  by eq.(4), the imaginary parts were extrapolated into the regions of large energies by assuming Gaussian tails.

The spectral properties of nucleons in asymmetric matter are best explored by keeping the total number density fixed to  $\rho = \rho_{eq}$ . Then, the average matrix element is  $(\overline{|M_{qq'}|^2})^{\frac{1}{2}} = 350 \text{ MeV fm}^3$ , being in agreement both with the derivation sketched above and reproducing the spectral functions of ref. [12].

In the imaginary part of the self-energies dynamical correlations are reflected most clearly and directly. Results for  $\text{Im}\Sigma_q \equiv \frac{1}{2}\Gamma_q$  are displayed in fig.4 for protons and neutrons ( $q=p,n$ ), respectively, at an asymmetry  $\xi = \frac{1}{4}$ . The overall dependence of  $\text{Im}\Sigma_q$  on energy is constrained by the requirement that the ground state is stationary. Theoretically, this is taken care off by using retarded Green functions, leading to  $\text{Im}\Sigma_q(\omega_F(q)) \equiv 0$  as seen in fig.5 and guaranteeing that the ground state is indeed stable as indicated by the vanishing width.

In Fig.5 also results from a recent Brueckner Hartree-Fock (BHF) study of the Tübingen group [7] are included. Both approaches agree qualitatively in the global energy dependence given by a strong increase of  $\text{Im}\Sigma_q$  at energies away from the Fermi surface. But in detail, differences are seen to emerge on the quantitative level and especially in the hole sector: While our approach predicts long tails of  $\text{Im}\Sigma_q$  extending to large values of  $|\omega - \omega_F|$  and eventually levelling off by slowly approaching asymptotic values, the BHF calculations show a much more pronounced fall off at energies deep in the Fermi sea. Such a cutoff behavior is somewhat unexpected at first sight because the density of intermediate ( $2h1p$ ) states still increases with increasing energy which should overcompensate the suppression introduced by the momentum structure of the interactions. The deviations in the particle sector ( $\omega > \omega_F$ ) are reflecting the differences in the interactions. The BHF calculations are based on the CD-Bonn NN-potential which seems to provide a larger amount of hard scattering at large off-shell momenta than our simplified description using a zero-range interaction, obviously not distinguishing between on- and off-shell processes. However, the results of ref.[7] show that similar differences are observed in the BHF calculations when using different NN-potentials. This points to an interesting - and rare - sensitivity of the dynamical self-energies on the off-shell momentum structure of interactions.

The striking similarity of our results to the full BHF calculations is a strong argument for the universality of the underlying dynamical effects. At first sight it might be surprising that the close relationship is obtained despite the fact that our approach does not include explicitly the tensor interaction. Tensor interactions play a crucial role in

BHF and also relativistic Dirac-BHF (DBHF) calculations [6]. The tensor interaction is of rank-2 in the spin and the orbital variables and as such has a vanishing expectation value for the ground state of spin saturated nuclear matter which we consider here. However, the tensor interaction contributes from second order on to the equation of state of symmetric and asymmetric nuclear matter. In the BHF and also the DBHF calculations the tensor parts introduce an especially strong proton-neutron correlation in the particle-particle channel [5, 6, 7]. Obviously, the on-shell part of that effect is accounted for by the phenomenological Skyrme functional but we cannot exclude that off-shell contributions might be missing.

A slightly different situation is encountered in the dynamical self-energies. As seen from eq.1, these self-energies are of at least second order in the residual interaction leading from the ground state to the intermediate excited states and back to the ground state. In these processes, the tensor interaction contributes in principle through the excitation of spin and spin-isospin modes in the particle-hole channel. However, since the corresponding particle-hole interactions are repulsive the spectral strengths of these modes are shifted to higher energies. Also, as seen in Fig.2 the interactions in the spin-isospin channels are relatively weak, inhibiting collective enhancements as observed in the spin-independent channels. Hence, the spectral properties close to the Fermi-surface are only weakly affected although contributions at higher energies and in the far off-shell regions cannot be excluded. Still, the close agreement with the BHF results of ref.[7] indicates that such effects cannot play a major role.

In free space the tensor interaction plays a crucial role in the proton-neutron system as reflected by the binding of the deuteron. In the present context one could expect a correlation in the particle-particle channel. However, explicit calculations by other groups have shown that such correlations die out quickly with increasing density. After all, the bulk properties of nuclei are well understood by nucleonic degrees of freedom without the need to introduce a significant amount neither of condensed deuteron matter nor *pn* pairing in the isospin  $I = 0$  channel, to the best of our knowledge. The reason is that the in-medium tensor interactions and, accordingly, the deuteron-like particle-particle channels are found to be suppressed with increasing densities [18, 19]. For example, the deuteron as a bound state disappears beyond the so-called Mott density [20, 21]. But as a reminder a pronounced *pn* correlation might survive at higher densities. As a side remark we note that the situation is different when investigating processes especially magnifying the in-medium pair channels like photo-absorption on nuclei above the giant dipole resonance where pair processes play a significant role (see e.g. [22]).

## B. Proton and Neutron Spectral Functions

In Fig. 6 proton and neutron spectral functions at  $\rho = \rho_{eq}$  are displayed for two different momenta and asymmetries  $\xi = \frac{1}{2}, \frac{1}{4}$ . In all cases, the quasiparticle peaks are clearly identified, as one would expect from symmetric nuclear matter. The main difference to symmetric nuclear matter are in fact the changes in the mean-field due to the isovector self-energy which translate into corresponding changes in the chemical potentials. With increasing neutron excess the protons are bound increasingly stronger while the effective neutron potential becomes shallower, leading to less binding. Thus, the number asymmetry induces via the isovector interactions a gap between the proton and neutron Fermi surfaces. Hence, both the shape and the location of the peak are influenced by the isovector interactions through their influence on the chemical potentials.

Comparing the results for  $\xi = \frac{1}{4}$  with those for symmetric matter,  $\xi = \frac{1}{2}$ , we find from Fig.6 that in asymmetric matter the proton hole strength functions are moved towards the Fermi level while the proton particle strength is moved away from the Fermi level. The neutron spectral distributions show the complementary behavior: the hole strength is shifted down into the Fermi sea while the particle strength is approaching the Fermi level. In neutron-rich matter the Fermi momentum for protons is smaller than in symmetric nuclear matter and for neutrons vice versa. We first consider the spectral functions in the hole sector, i.e. for states in the Fermi sphere  $k_q \leq k_{Fq}$ . The hole spectral functions peak are close the mean-field on-shell energy position

$$\omega_{on}^q = \frac{\hbar k^2}{2m_q^*} + U_q^{eff} - \omega_{fq} = \frac{\hbar(k^2 - k_{Fq}^2)}{2m_q^*}. \quad (28)$$

For a momentum of  $k = 31.3 \text{ MeV}/c$  this leads to a proton quasiparticle peak at about  $\omega_{on}^p = -28 \text{ MeV}$ , while the neutron quasiparticle position is at  $\omega_{on}^n = -78 \text{ MeV}$ , as seen in Fig.6. Hence, the proton peak is clearly shifted towards the Fermi edge, while the neutron strength is repelled. Similar observations are made in the particle sector. For  $k = 312.5 \text{ MeV}/c$ , corresponding to  $\omega(p) = 35 \text{ MeV}$  and  $\omega(n) = 8 \text{ MeV}$  respectively, the quasiparticle peak for the neutron is shifted towards the Fermi level, while the quasiparticle peak for the neutron is shifted away.

Another observation from Fig.6 is that the width of the quasi-particle peaks decreases when approaching the Fermi surface. This is in agreement with the general expectation that closer to the Fermi surface the life time of quasi-particle states increases strongly. The energy-momentum structure of  $\Gamma(\omega, k)$  is illustrated in Fig.4 for two momentum

cuts in symmetric and asymmetric matter. From the behavior of  $\Gamma(\omega, k)$  we conclude that in asymmetric matter the collision rates in the hole sector increase for neutrons while for protons they slightly decreases. For either type of nucleon the amount of correlations decrease for states above the Fermi level compared to symmetric matter. These results indicate that the real and imaginary parts of the polarization self-energies roughly scale with the density of states of the same kind of particles. Similar observation have been made in [7].

The dependence of spectral functions in nuclear matter on density is investigated in Fig.7 and Fig.8. Spectral functions for symmetric matter and at total densities between half and twice nuclear saturation density  $\rho_{eq} = 0.16 \text{ fm}^{-3}$  are displayed. The results are obtained by using the density dependent matrix element from equation 27. In Fig.7 the spectral distributions of a nucleon well inside the Fermi sea are displayed. The evolution of the spectral functions with density reflect the changes in the chemical potentials. At  $\rho = \frac{1}{2}\rho_{eq}$  a state with the chosen momentum is much closer to the Fermi surface than for  $\rho = \rho_{eq}$  or  $\rho = 2\rho_{eq}$ . This explains the variation in width and position of the quasi-particle peak seen in Fig.7, seen to be shifted into the Fermi sea with a considerable gain of width and high energy strength when the density increases.

In Fig.8 spectral functions for a particle state well above the Fermi surface are shown. Here, a complementary behavior is found. With increasing density the relative distance of the quasi-particle from the Fermi surface decreases which is reflected in a reduction of the energy shift and the width of the quasi-particle peak at higher density. In both cases, long spectral tails in the region below or above the Fermi surface, respectively, are found, indicating a considerable shift of single particle strength away from the quasi-particle peak. The overall features, however, are qualitatively similar to those observed previously in symmetric nuclear matter [2, 3] although the results differ on the quantitative level.

### C. Proton and Neutron Momentum Distribution

We finally consider the proton and neutron one-body ground state momentum distributions

$$n_q(k) = \int_{-\infty}^{\mu_q} d\omega a_q(\omega, k) \quad (29)$$

where  $\mu_q$  is the chemical potential for nucleons of type  $q = p, n$ . Results for symmetric and asymmetric nuclear matter are shown in Fig.9. There, the shrinking of the proton Fermi sphere in neutron-rich matter is clearly visible in terms of the diminished region of occupied proton momentum states. In asymmetric matter the structure of the momentum distributions follows otherwise closely the same pattern as found already in symmetric matter: Inside the Fermi sea the occupancy is reduced by about 10% and this fraction of the spectral strength is shifted into a high momentum tail with an almost exponential decline. At first sight it seem surprising to find that at high momenta the distributions approach the each other showing very similar magnitudes and slopes. This result is another illustration of the universality of the dynamical short range correlations which already was found in our previous investigations [2, 3, 4]. The bulk parts of proton and neutron matter are seen to be contained in regions  $k \leq k_F(q)$ , where obviously,  $k_F(p) \leq k_F(n)$  in neutron-rich matter. The short range correlations produce a similar pattern as in symmetric matter by depopulating the Fermi sea by about 10% irrespective of the asymmetry. In fact in all cases the high momentum tails are almost identical, thus confirming the universality of the underlying dynamical processes.

Integrating the proton and neutron momentum-distributions over a sphere with radius  $k$  in momentum-space and normalizing the result to the density we obtain the cumulative density index

$$x_q(k) = \frac{1}{\rho_q \pi^2} \int_0^k dk' n_q(k') k'^2 \quad (30)$$

where  $x_q(k) \rightarrow 1$  for  $k \rightarrow \infty$ . The quantity  $x_q$  is particular well suited to display the fractional relative exhaustion of the given density up to a finite momentum  $k$ . For a system of non-interacting quasi-particles we expect  $x_q(k) \sim (\frac{k}{k_F})^3 \theta(k_F - k) + \theta(k - k_F)$ . In a system with correlations the Fermi surface will be visible as a discontinuity in the slope as seen in Fig.10. The results displayed in Fig.10 show very directly the significant difference in the correlations pattern of protons and neutrons: A large fraction of the proton strength is shifted into the high momentum region as indicated by the slow convergence of  $x_p(k)$  towards unity. For symmetric nuclear matter we find from equation 30 that about 82% of the states in the Fermi sphere ( $k \leq k_{Fq}$ ) are occupied, while in neutron-rich matter with  $\xi = \frac{1}{4}$  only 71% of the proton but 87% of the neutron states inside the Fermi sphere are occupied. This observation is on a qualitative level in agreement with BHF calculations [7]. Interestingly, we have obtained the asymmetric depletion of proton and neutron occupation without using explicitly a tensor interaction.

#### IV. SUMMARY AND OUTLOOK

Dynamical correlations in asymmetric infinite nuclear matter were investigated in a transport theoretical approach, thereby extending our previous work into a new regime. It is worthwhile to emphasize that only few studies on dynamical correlations in asymmetric exist. In asymmetric matter isovector effects are strongly enhanced with increasing asymmetry. On the mean-field level this was taken into account by using a modern Skyrme energy density functional from the Lyon group [17] with parameters adjusted both to finite nuclei and neutron stars. In this sense, we describe the evolution of mean-field dynamics with asymmetry and density in a realistic model. In particular, the saturation properties of infinite nuclear matter are well described. Using Landau-Migdal theory we could derive from the Skyrme functional the corresponding effective quasi-particle interaction in a self-consistent way. An approach was presented which allows to extract the short-range interactions by subtracting the pion exchange contributions.

The overall features of self-energies and spectral functions in asymmetric nuclear matter resemble those found in our previous work on short range correlations in symmetric matter. In particular, the present investigation confirms our previous conjecture on the universal character of short range correlations in infinite nuclear matter. An interesting observation in the present context is the sensitivity of the spectral distributions on the momentum structure of self-energies and interactions.

#### Acknowledgments

We thank F. Frömel for helpful discussions and numerical hints during preparation of this work.

#### APPENDIX A: LANDAU-MIGDAL PARAMETERS FOR THE PION

Second variation of the energy density in equation (16) with respect to spin and isospin densities leads to

$$\begin{aligned} \frac{\partial^2 E_\pi(\rho)}{\partial \rho_q \partial \rho_{q'}} &= \sum_{S,T=0,1} [V_{ST}(k_f(q), k_f(q')) (\vec{\sigma}_1 \cdot \vec{\sigma}_2)^S (\vec{\tau}_1 \cdot \vec{\tau}_2)^T \\ &+ \frac{1}{k_f(q')^2} \sum_{q''} \int dk k^2 \Theta(k_f(q'') - k) \frac{\partial}{\partial q} V_{ST} < (\vec{\sigma}_1 \cdot \vec{\sigma}_2)^S (\vec{\tau}_1 \cdot \vec{\tau}_2)^T >] \end{aligned} \quad (\text{A1})$$

where the brackets indicate ground state expectation values. From which we now identify the Landau-Migdal parameters:

$$f^{(\pi)} = N_0(k_f) V_{00} + f^r(k_f) \quad (\text{A2})$$

$$f'^{(\pi)} = N_0(k_f) V_{10} \quad (\text{A3})$$

$$g^{(\pi)} = N_0(k_f) V_{01} \quad (\text{A4})$$

$$g'^{(\pi)} = N_0(k_f) V_{11} \quad (\text{A5})$$

where  $f^r(k_f)$  is an rearrangement term, which appears for spin-saturated symmetric nuclear matter only in the  $S = 0$ ,  $T = 0$  channel. Expansion of the in-medium scattering amplitude in a Legendre series, which is common, leads to

$$f_l^{(\pi)} = \frac{1}{2} \int_{-1}^1 P_l(\cos \theta) f^\pi(\cos \theta) d\cos \theta. \quad (6)$$

The integration over the angle  $\theta$  is done using the Newman formula

$$Q_l(t) = \frac{1}{2} \int_{-1}^1 \frac{P_l(x)}{t - x} dx \quad (7)$$

where the  $Q_l(t)$  are Legendre polynomials of the 2nd kind. Using equation (7) together with our expressions for the Landau-Migdal parameters leads to

$$f_l^{(\pi)} = -4\pi \frac{9}{4} N_0(k_F) \frac{f_\pi^2}{2k_F^2} Q_l(1 + \frac{m_\pi^2}{2k_F^2}) + f_l^{(r)}(k_F) \quad (8)$$

$$f_l'^{(\pi)} = 4\pi \frac{3}{4} N_0(k_F) \frac{f_\pi^2}{2k_F^2} Q_l(1 + \frac{m_\pi^2}{2k_F^2}) \quad (9)$$

$$g_l^{(\pi)} = 4\pi \frac{3}{4} N_0(k_F) \frac{f_\pi^2}{2k_F^2} Q_l(1 + \frac{m_\pi^2}{2k_F^2}) \quad (10)$$

$$g_l'^{(\pi)} = g'_H \delta_{l0} - 4\pi \frac{1}{4} N_0(k_F) \frac{f_\pi^2}{2k_F^2} Q_l(1 + \frac{m_\pi^2}{2k_F^2}). \quad (11)$$

where the  $l = 0$  components in the  $S = 1, T = 1$  channel includes in addition the direct (i.e. Hartree-type) contributions

$$g'_H = 4\pi N_0(k_F) \frac{f_\pi^2}{m_\pi^2} \quad (12)$$

For the additional rearrangement term in equation (8) we get

$$f^{(r)}(k_F) = N_0(k_F) \frac{1}{k_F^2} \int dk k^2 \Theta(k_F - k) \frac{\partial}{\partial q} V_0^{(\pi)}(k, k') \quad (13)$$

where  $V_0^\pi(k, k')$  is the monopol component of the  $S = 0, T = 0$  u-channel pion exchange interaction.

---

[1] W. Dickhoff, C. Barbieri, *Prog.Part.Nucl.Phys.* **52** (2004) 377-496.

[2] J. Lehr, M. Effenberger, H. Lenske, S. Leupold, U. Mosel, *Phys. Lett.* **B483** (2000) 324.

[3] J. Lehr, H. Lenske, S. Leupold, U. Mosel, *Nucl. Phys.* **A703** (2002) 393.

[4] F. Froemel, H. Lenske, U. Mosel, *Nucl. Phys.* **A723** (2003) 544.

[5] P. Bozek, *Phys. Lett.* **B586** (2004) 239-243.

[6] F. de Jong and H. Lenske, *Phys. Rev.* **C54** (1996) 1488.

[7] Kh.S.A. Hassaneen, H. Müther, *Phys. Rev.* **C70** (2004) 054308; arXiv:nucl-th/0408035.

[8] D. Cortina-Gil, T. Baumann, H. Geissel, K. Sümerer, L. Axelson, U. Bergmann, M.J.G. Borge, L. Fraile, M. Hellström, M. Ivanov, N. Iwasa, R. Janik, B. Jonson, H. Lenske, K. Markenroth, G. Münzenberg, F. Nickel, T. Nilsson, A. Ozawa, K. Riisager, G. Schrieder, W. Schwab, H. Simon, C. Scheidenberger, B. Sitar, M. Smedberg, P. Strmen, T. Suzuki, M. Winkler, *Eur.Phys.J* **A10** 49 (2001).

[9] D. Cortina-Gil, K. Markenroth, F. Attallah, T. Baumann, J. Benlliure, M.J.G. Borge, L.V. Chulkov, U. Datta Pramanik, J. Fernandez-Vazquez, C. Forssn, L.M. Fraile, H. Geissel, J. Gerl, F. Hammache, K. Itahashi, R. Janik, B. Jonson, S. Karlsson, H. Lenske, S. Mandal, M. Meister, X. Mocko, G. Mnzenberg, T. Ohtsubo, A. Ozawa, Y. Parfenova, V. Pribora, K. Riisager, H. Scheit, R. Schneider, K. Schmidt, G. Schrieder, H. Simon, B. Sitar, A. Stolz, P. Strmen, K. Sümerer, I. Szarka, S. Wan, H. Weick and M. Zhukov, *Phys.Lett.* **B529** (1-2) (2002) pp. 36-41.

[10] H. Lenske, F. Hofmann, C.M. Keil, *Rep.Prog.Nucl.Part.Phys.* **46** (2001) 187, e-Print Archive: nucl-th/0012082.

[11] H. Lenske, C.M. Keil, Nadia Tsoneva, *Prog.Part.Nucl.Phys.* **53** (2004) 153.

[12] O. Benhar, A. Fabrocicini, S. Fantoni, *Nucl. Phys.* **A505** (1989) 267; O. Benhar, A. Fabrocicini, S. Fantoni, *Nucl. Phys.* **A550** (1992) 741.

[13] L.P. Kadanoff and G. Baym, *Quantum Statistical Mechanics* (Benjamin, New York, 1962).

[14] A. B. Migdal, *Theory of Finite Fermi Systems and Applications to Atomic Nuclei* (Interscience, New York, 1975).

[15] M. Bender, J. Dobaczewski, J. Engel, W. Nazarewicz, *Phys. Rev.* **C85** (2002) 054322.

[16] I. Bombaci, U. Lombardo *Phys. Rev.* **C44** (1991) 1892.

[17] E. Chabanat, P. Bonche, P. Haensel, J. Meyer, R. Schaeffer, *Nucl. Phys.* **A627** (1997) 710.

[18] G. Röpke, A. Schnell, P. Schuck, U. Lombardo, *Phys.Rev.* **C61** (2000) 024306.

[19] L. Zamick, D. C. Zheng, and M. S. Fayache, *Phys. Rev. C* **51**, 1253 (1995); M. S. Fayache and L. Zamick, *Phys. Rev. C* **51**, 160 (1995)

[20] G. Röpke, L. Münchow, and H. Schulz, *Nucl. Phys.* **A379**, 536 (1982); *Phys. Lett. B* **110**, 21 (1982); G. Ropke, M. Schmidt, L. Münchow, and H. Schulz, *Nucl. Phys.* **A399**, 587 (1982).

[21] M. Schmidt, G. Röpke, and H. Schulz, *Ann. Phys. (NY)* **202**, 57 (1990).

[22] O. Benhar, A. Fabrocini, S. Fantoni, A. Yu. Illarionov, G. I. Lykasov, *Phys.Rev.* **C67** (2003) 014326

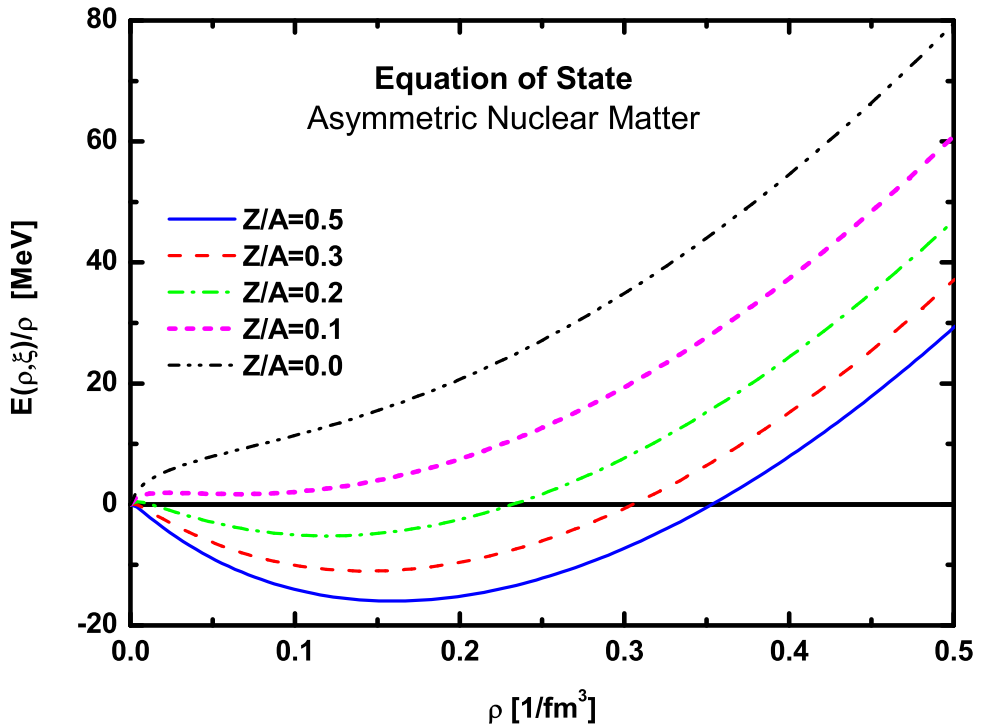


FIG. 1: Equation of state of infinite nuclear matter at various asymmetries  $\xi = \rho_p/\rho = Z/A$ . Results obtained with the Lyon-4 parameter set [17] are shown.

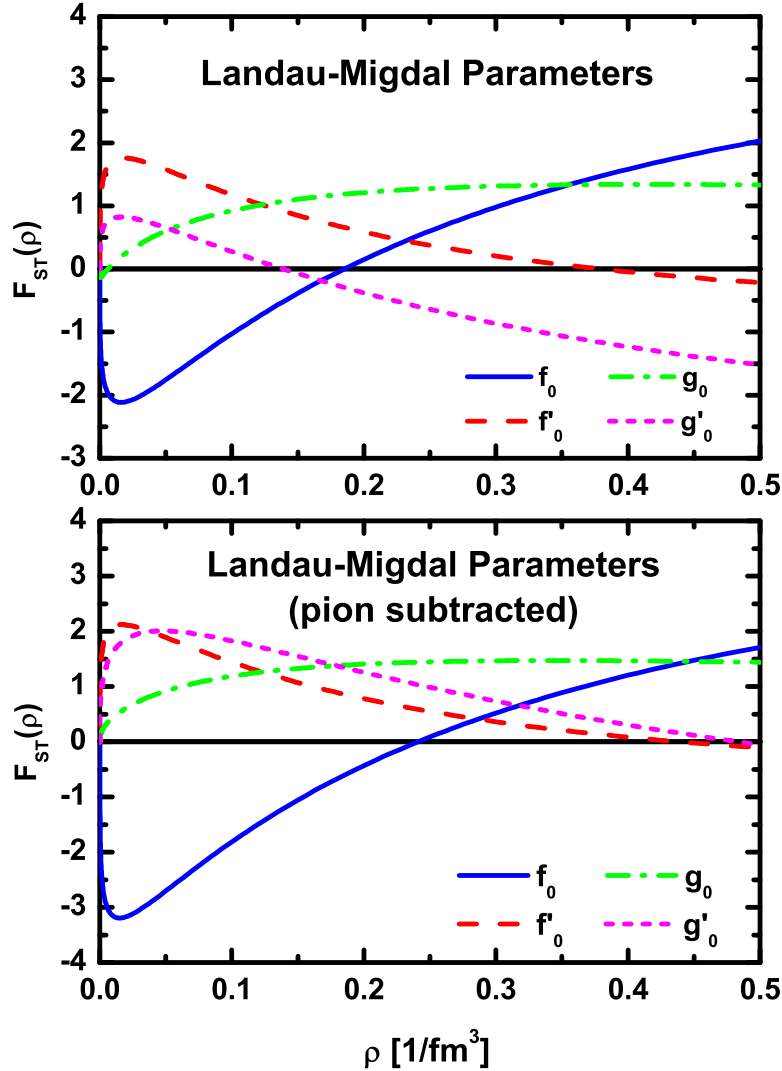


FIG. 2: Landau-Migdal parameters in symmetric nuclear matter for the full Lyon-4 interaction (upper panel) [17] and the pion-subtracted short range interaction (lower panel).

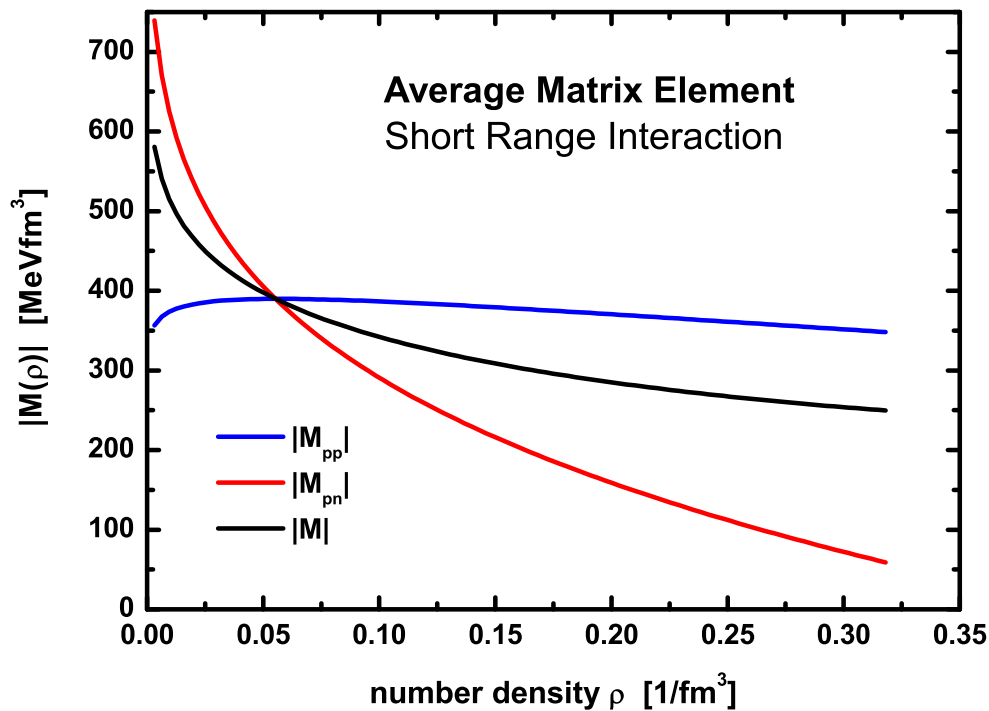


FIG. 3: Dependence of the average short range interaction matrix elements  $|M_{qq'}$  and of the average matrix element  $\overline{M}$ , eq.27, on density in infinite nuclear matter.

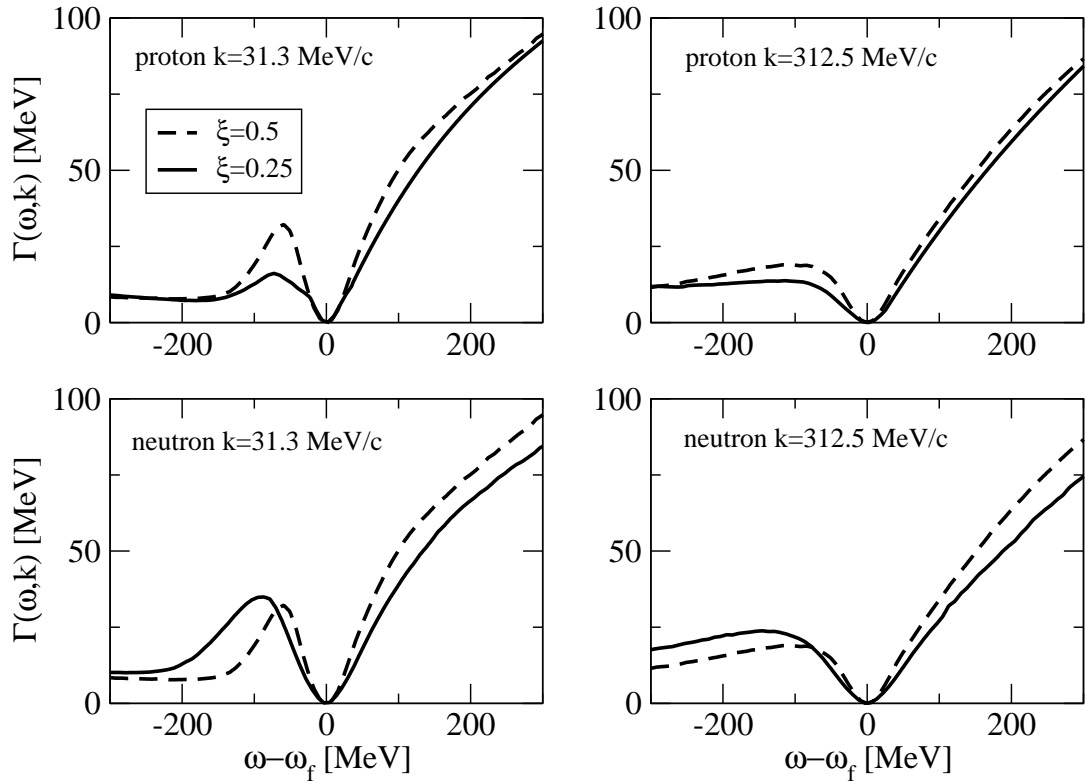


FIG. 4: The nucleon width for symmetric (dashed line) and asymmetric nuclear matter (full line). The upper graphs refer to protons the lower ones to neutrons.

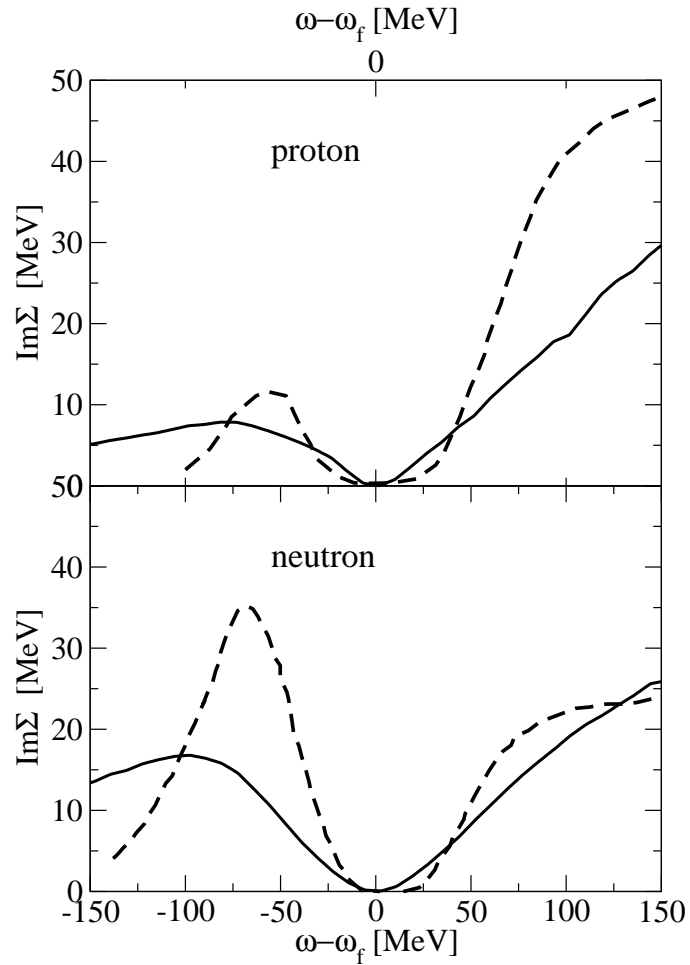


FIG. 5: The imaginary part of the nucleon self-energy for momentum  $k = 0.4k_f$  and asymmetry  $\xi = 0.25$  at a density  $\rho = 0.17$   $1/fm$ . The dotted line represents the BHF results from [7].

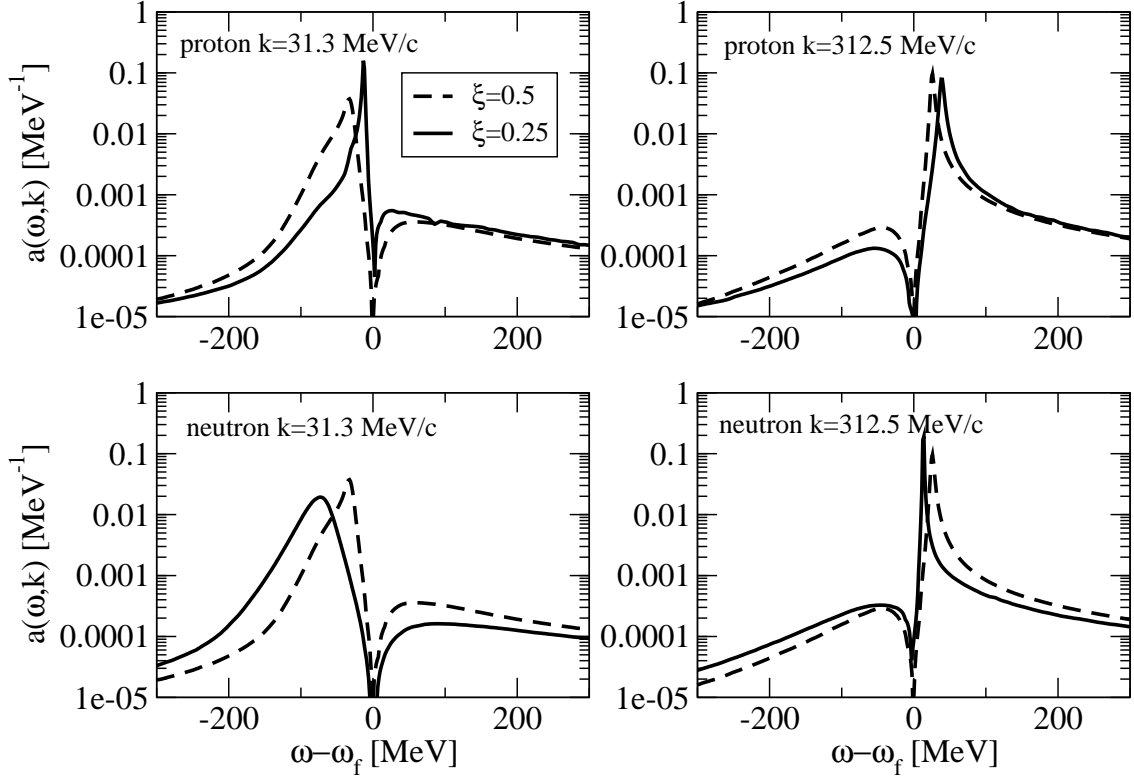


FIG. 6: The nucleon spectral function for symmetric and asymmetric nuclear matter. The dashed line refers to symmetric and the straight line to asymmetric nuclear matter with an asymmetry of  $\xi = 0.25$ . The upper graphs show the results for protons, the lower ones the results for neutrons.

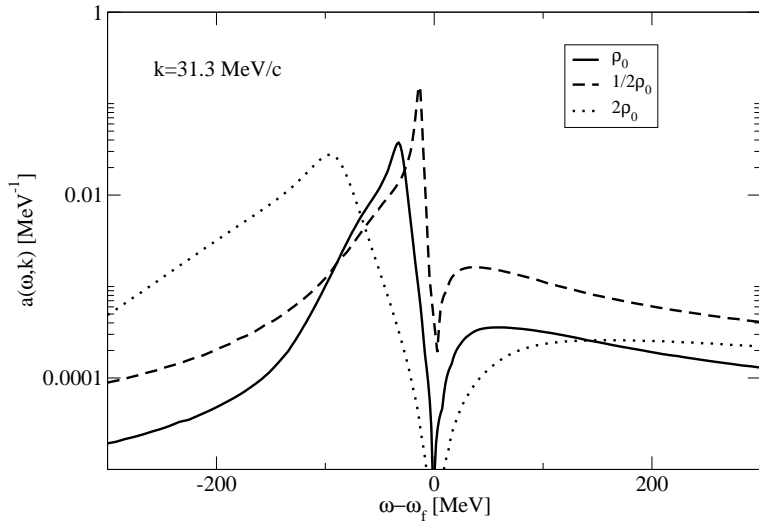


FIG. 7: Spectral functions of a nucleon well inside the Fermi sea at density  $\rho = \frac{1}{2}\rho_{eq}$ ,  $\rho = \rho_{eq}$  and  $\rho = 2\rho_{eq}$ .

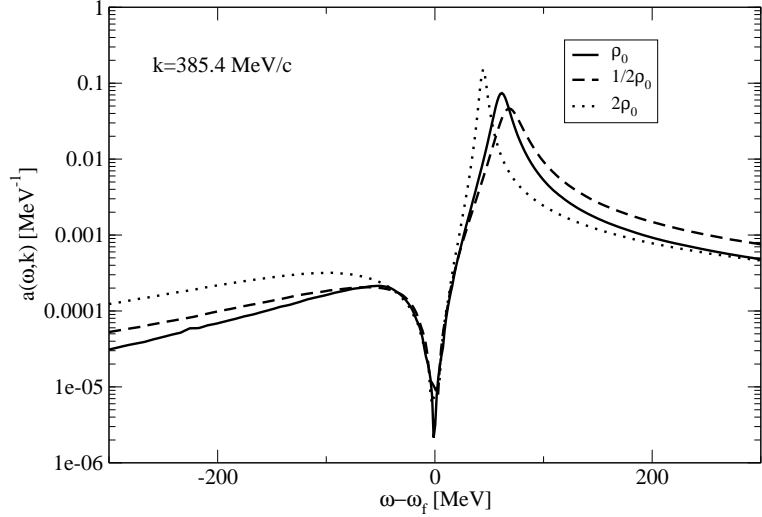


FIG. 8: Spectral functions of a nucleon well outside the Fermi sea at density  $\rho = \frac{1}{2}\rho_{eq}$ ,  $\rho = \rho_{eq}$  and  $\rho = 2\rho_{eq}$ .

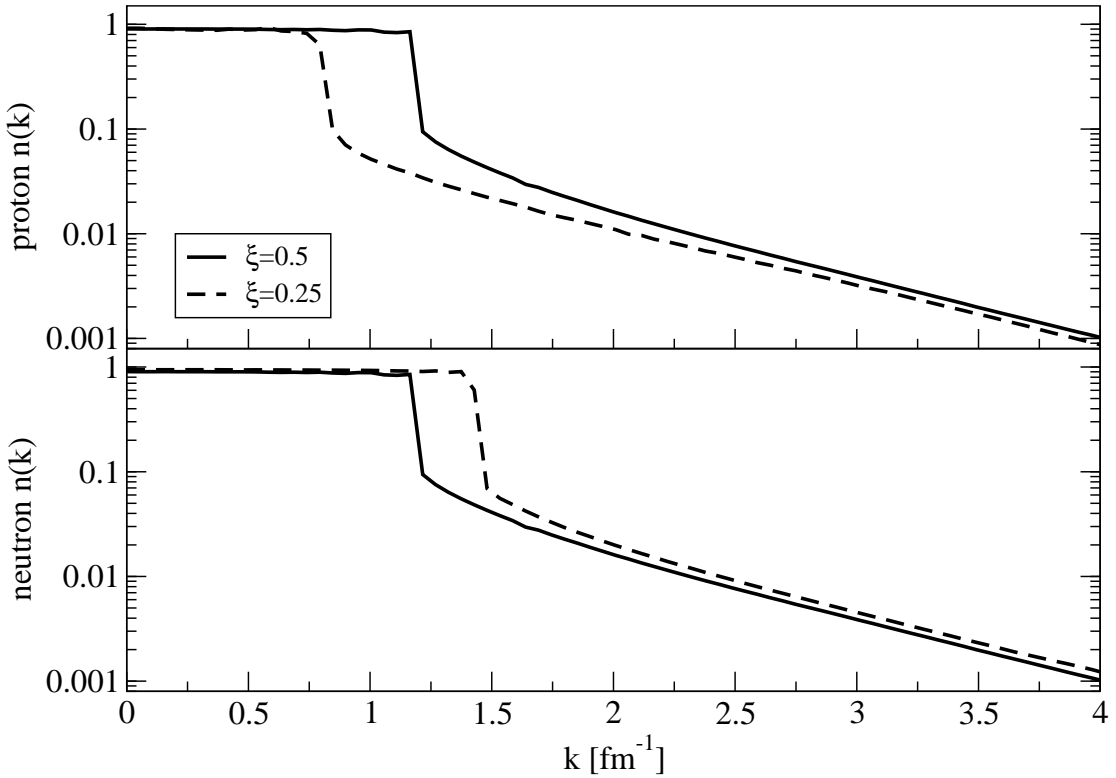


FIG. 9: The momentum distribution for protons (upper graph) and neutrons (lower graph). The straight line is the result for symmetric nuclear matter the dashed line for asymmetric nuclear matter ( $\xi = 0.25$ )

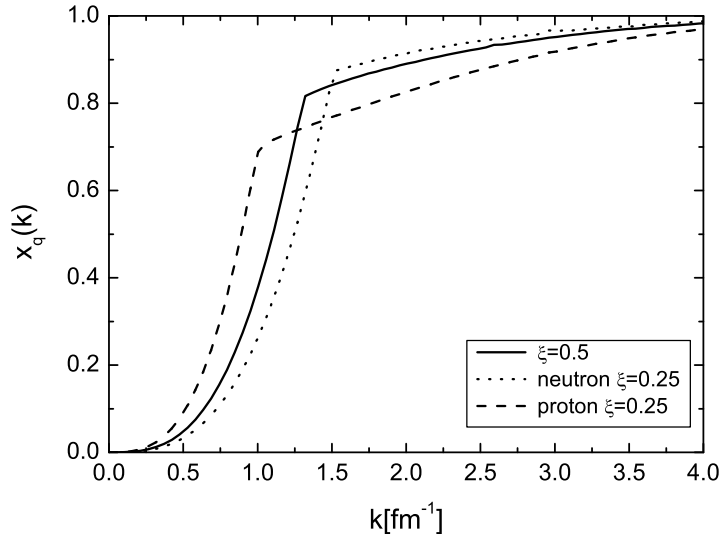


FIG. 10: The the cumulative density index for symmetric nuclear matter (full line) and for protons (dashed line) and neutrons (dotted line) in neutron-rich matter with  $\xi = 0.25$ .